MOLECULAR AND CELLULAR BIOLOGY, Nov. 1999, p. 7712–7723 Vol. 19, No. 11
0270-7306/99/$04.00+0


# Characterization of a Vacuolar Pyrophosphatase in *Trypanosoma brucei* and Its Localization to Acidocalcisomes

CLAUDIA O. RODRIGUES, DAVID A. SCOTT, AND ROBERTO DOCAMPO*

*Laboratory of Molecular Parasitology, Department of Pathobiology, University of Illinois at Urbana-Champaign, Urbana, Illinois 61802*

Received 25 May 1999/Returned for modification 19 July 1999/Accepted 23 August 1999

**Inorganic pyrophosphate promoted the acidification of an intracellular compartment in permeabilized procyclic trypomastigotes of *Trypanosoma brucei*, as measured by acridine orange uptake. The proton gradient generated by pyrophosphate was collapsed by addition of nigericin or $NH_4Cl$. Pyrophosphate-driven proton translocation was stimulated by potassium ions and inhibited by KF, by the pyrophosphate analogs imidodiphosphate and aminomethylenediphosphonate (AMDP), and by the thiol reagent *p*-hydroxymercuribenzoate at concentrations similar to those that inhibit the plant vacuolar $H^+$-pyrophosphatase (PPase). The proton translocation activity had a pH optimum around 7.5 and was partially inhibited by 7-chloro-4-nitrobenz-2-oxa-1,3-diazole (10 μM) and unaffected by bafilomycin $A_1$ (40 nM), concanamycin A (5 nM), sodium *o*-vanadate (500 μM), oligomycin (1 μM), *N*-ethylmaleimide (100 μM), and $KNO_3$. AMDP-sensitive pyrophosphate hydrolysis was detected in both procyclic and bloodstream trypomastigotes. Measurements of acridine orange uptake in permeabilized procyclic trypomastigotes in the presence of different substrates and inhibitors suggested the presence of $H^+$-ATPase, $H^+$-PPase, and (ADP-dependent) $H^+/Na^+$ antiport activity in the same compartment. Separation of bloodstream and procyclic trypomastigote extracts on Percoll gradients yielded fractions that contained $H^+$-PPase (both stages) and $H^+/Na^+$ exchanger (procyclics) activities but lacked markers for mitochondria, glycosomes, and lysosomes. The organelles in these fractions were identified by electron microscopy and X-ray microanalysis as acidocalcisomes (electron-dense vacuoles). These results provide further evidence for the unique nature of acidocalcisomes in comparison with other, previously described, organelles.**

African trypanosomiasis (sleeping sickness), caused by the *Trypanosoma brucei* group of parasitic protozoa, occurs in 36 countries in sub-Saharan Africa, where it is a public health problem with a major impact on social and economic development. It has been estimated that about 300,000 new cases occur annually (41). In addition, *T. brucei* causes a similar disease in livestock, thereby making a large part of the African continent unsuitable for agricultural development. There is therefore considerable interest in developing novel chemotherapy, based on unique aspects of the structure and metabolism of these early-branching eukaryotes.

Organelle acidification is an essential function in eukaryotes. Acidification is required for lysosomal enzyme activity, for uncoupling of endocytosed ligands from receptors, and to provide a driving force (via $H^+$ or membrane potential gradients) for uptake of solutes such as biogenic amines, sugars, amino acids, and cations (3, 15, 16, 28).

In all eukaryotic cells, acidification is driven by ATPases of the vacuolar type (V-$H^+$-ATPases; 15). Additionally, some cell types have $H^+$ pumps which are driven by pyrophosphate ($PP_i$). Apart from isolated reports on *Saccharomyces carlsbergensis* (22) and rat liver Golgi vesicles (4), vacuolar $H^+$-pyrophosphatases (V-$H^+$-PPases) had, until recently, been found only in vacuoles of plants, ranging from the unicellular alga *Acetabularia* to higher plants (18, 33), although there is a homologous $H^+$-$PP_i$ synthase located in chromatophores in phototrophic bacteria (1).

* Corresponding author. Mailing address: Laboratory of Molecular Parasitology, Department of Pathobiology, College of Veterinary Medicine, University of Illinois at Urbana-Champaign, 2001 South Lincoln Ave., Urbana, IL 61802. Phone: (217) 333-3845. Fax: (217) 244-7421. E-mail: rodoc@uiuc.edu.

The known range of organisms possessing V-$H^+$-PPases was recently greatly expanded by our discovery of this activity in *Trypanosoma cruzi* (38). One of the key questions we addressed in that work was the location of the V-$H^+$-PPase, which had to be different from that in plants, as trypanosomatids lack a plant-like central vacuole. Our results showed that much of the activity was associated with a vesicle rich in calcium, phosphorus, and magnesium, which we had previously identified as the acidocalcisome (37). This organelle was first described as the inclusion vacuole in *Trypanosoma cyclops* (45).

We initially defined the acidocalcisome in intact or permeabilized *T. brucei* (35, 42) functionally as an organelle that was acidic and that imported $Ca^{2+}$ by the action of a vanadate-sensitive $Ca^{2+}$-ATPase. Acidity appeared to be generated and sustained by a bafilomycin $A_1$-sensitive V-$H^+$-ATPase and was important for $Ca^{2+}$ retention, since alkalinization induced by nigericin, $NH_4Cl$, or bafilomycin $A_1$ treatment was followed by $Ca^{2+}$ release (35, 42–44). $Na^+$ was shown to collapse ATP-induced proton gradients and to induce release of $Ca^{2+}$ (43, 44). The latter effect was not additive with the $Ca^{2+}$-releasing effects of nigericin, implying that an $Na^+/H^+$ antiport activity is also associated with acidocalcisomes (43, 44). This activity was inhibited by the antioxidant 3,5-dibutyl-4-hydroxytoluene but unaffected by amiloride analogs (43, 44).

Subsequently, acidocalcisomes were detected in other trypanosomatids, i.e., *T. cruzi* (12, 37) and *Leishmania amazonensis* (23), and in the apicomplexan parasite *Toxoplasma gondii* (30). As X-ray microanalysis of unfixed cryosections of *T. cruzi* epimastigotes indicated the presence of calcium within the inclusion vacuoles, we inferred that these were the acidocalcisomes (37). An acidic interior for these organelles was suggested by an increase in their potassium content after treatment with the $K^+/H^+$ ionophore nigericin (37). This is sup-

ported by results from *T. brucei*, where use of weak bases, which can cause swelling of acidic vesicles, had this effect on inclusion vacuoles (7). Subsequently, as noted above, we found that the $H^+$-PPase is associated with the calcium- and phosphorus-containing organelles. These demonstrated a unique density, being much more dense even than the most dense organelle previously found in trypanosomatids, the glycosome (38).

In this work, we found that both bloodstream and procyclic trypomastigotes of *T. brucei* possess a V-$H^+$-PPase with features in common with the *T. cruzi* and plant activities and used this activity as a marker for the purification of acidocalcisomes. The purified organelles were shown to possess $Na^+/H^+$ exchange activity and to generate a $PP_i$-dependent membrane potential. In permeabilized cells, it was confirmed that $Na^+$ could diminish proton gradients established via $H^+$-ATPase activity. $Na^+$ had the same effect on $PP_i$-generated proton gradients if ADP was present. Together, these data suggest the colocalization of $H^+$-ATPase and $H^+$-PPase activities and provide evidence that the isolated acidocalcisome is the same organelle as that identified initially on a functional basis.

(This work was presented in partial fulfillment of the requirements for the Ph.D. thesis of C.O.R.)

## MATERIALS AND METHODS

**Culture methods.** *T. brucei* procyclic forms (ILTar 1 or MITat. 1.4 procyclics) were grown at 28°C in medium SDM-79 (5) supplemented with 10% heat-inactivated fetal calf serum. At 2 to 3 days after inoculation, the cells were collected by centrifugation, washed twice in 0.25 M sucrose, and resuspended in the same solution before use in experiments. *T. brucei* bloodstream forms (monomorphic strain 427 from clone MITat 1.4, otherwise known as variant 117) were isolated from infected mice or rats as described previously (10). The final concentration of cells was determined by using a Neubauer chamber. Protein (except for Percoll fractions [see below]) was measured by using the Bio-Rad Coomassie blue method.

**Chemicals.** Aprotinin, ADP, ATP, digitonin, dithiothreitol, Dulbecco's phosphate-buffered saline, imidodiphosphate (IDP), leupeptin, *N*,*N*′-dicyclohexylcarbodiimide, nigericin, valinomycin, ADP, ATP, 7-chloro-4-nitrobenz-2-oxa-1,3-diazole, sodium orthovanadate, pepstatin, *p*-hydroxymercuribenzoate, phenylmethylsulfonyl fluoride, carbonyl cyanide *p*-trifluoromethoxyphenylhydrazone (FCCP), and sodium $PP_i$ were purchased from Sigma Chemical Co., St. Louis, Mo. Bafilomycin $A_1$ and concanamycin A were from Kamiya Biomedicals, Thousand Oaks, Calif. Acridine orange, Oxonol VI, 2-amino-6-mercapto-7-methylpurine ribonucleoside (MESG), purine nucleoside phosphorylase (PNP), and the standard phosphate solution were from Molecular Probes, Eugene, Oreg. Aminomethylenediphosphonate (AMDP) (50) was kindly provided by Philip Rea, University of Pennsylvania. All other reagents were analytical grade.

**Proton pump activity.** $PP_i$-driven proton transport was assayed by measuring changes in the absorbance of acridine orange ($A_{493} - A_{530}$) in an SLM-Aminco DW 2000 dual-wavelength spectrophotometer (38). Cells were incubated at 30°C in 2.5 ml of standard 65 mM KCl–125 mM sucrose buffer (pH 7.2) or alternate buffers (see Table 3), containing, in addition, 2 mM $MgSO_4$, 10 mM HEPES, 50 μM EGTA, 3 μM acridine orange, 16 μM digitonin (for permeabilized-cell experiments or to test the effect of digitonin on isolated cell fractions), and different inhibitors where indicated, for 3 min prior to the addition of 0.1 mM $PP_i$ (pH 7.2). Each experiment with permeabilized cells was repeated at least three times with different cell preparations, and the figures show representative experiments.

**$PP_i$ assay.** $PP_i$ activity in terms of phosphate release was assayed as described by Scott et al. (38). Reaction mixtures contained 65 mM KCl, 125 mM sucrose, 10 mM K-HEPES, 2 mM $MgSO_4$, 50 μM EGTA at pH 7.2 (or other buffers [see Table 3]), 0.1 mM MESG, 0.4 U of PNP per ml, and a cell membrane preparation in a total volume of 1.0 ml. Activity was monitored by determining the increase in absorbance ($A_{355} - A_{330}$) with a DW2000 spectrophotometer at 30°C and was calibrated in each buffer with a standard phosphate solution. Membranes were prepared by lysing cells suspended in a buffer containing 125 mM sucrose, 20 mM Tris-HEPES (pH 7.4), and protease inhibitors (leupeptin at 1 μg/ml, pepstatin at 1 μg/ml, aprotinin at 1 μg/ml, and 1 mM phenylmethylsulfonyl fluoride) by sonication, followed by three washes (each for 2 min at 2,800 × *g*) and final resuspension of the membrane pellet in 0.25 M sucrose.

**Membrane potential measurements.** Membrane potential was monitored by measuring the increase in absorbance of Oxonol VI (1 μM) ($A_{630} - A_{596}$) (46) in a DW2000 spectrophotometer, in the standard buffer described for the proton transport measurements, at 30°C. Oxonol VI has been shown to be a valid indicator for measurement of the membrane potential generated by $PP_i$-dependent proton translocation in plant tonoplasts (26).

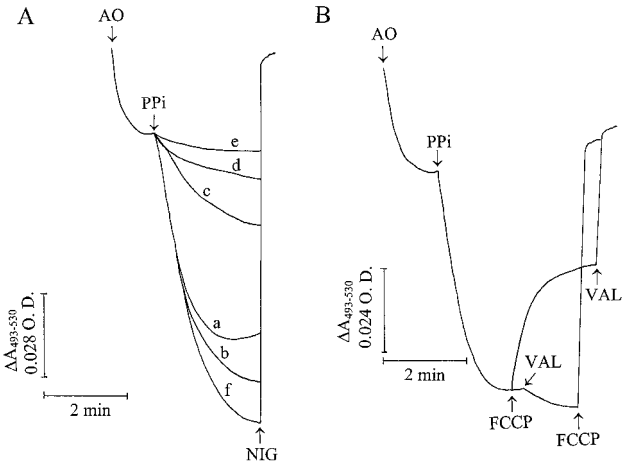


FIG. 1. $PP_i$-driven proton transport in permeabilized procyclic trypomastigotes and effects of ionophores. (A) Procyclic trypomastigotes (0.1 mg of protein/ml) were added to different buffers containing 2 mM $MgSO_4$, 50 μM EGTA, and 10 mM HEPES (pH 7.2); 16 μM digitonin; and, in addition, 65 mM KCl–125 mM sucrose (trace a), 130 mM KCl (trace b), 65 mM NaCl–125 mM sucrose (trace c), 130 mM NaCl (trace d), 65 mM *N*-methylglucamine chloride (trace e), and 65 mM KCl–65 mM NaCl (trace f). Acridine orange (AO) at 3 μM, 0.1 mM $PP_i$, and 5 μM nigericin (NIG) were added where indicated by the arrows (nigericin was added in all of the experiments, but only one line is indicated for clarity since the traces were superimposable). (B) Procyclic trypomastigotes (0.1 mg of protein/ml) were added to a buffer containing 65 mM KCl, 125 mM sucrose, 2 mM $MgSO_4$, 50 μM EGTA, 10 mM HEPES (pH 7.2), and 16 μM digitonin. Acridine orange (3 μM), $PP_i$ (0.1 mM), FCCP (1 μM), and valinomycin (VAL; 1 μM) were added where indicated by the arrows. O.D., optical density.

**Subcellular fractionation.** Subcellular fractionation was performed as described previously (38). Collected fractions were assayed for $PP_i$-driven proton transport, PPase (phosphate release) activity, general ATPase activity, and markers of mitochondria (isocitrate dehydrogenase), glycosomes (hexokinase), lysosomes (α-mannosidase), and plasma membrane (α-glucosidase). Proton transport was measured as described above, except that the standard buffer for *T. brucei* bloodstream forms contained 130 mM KCl instead of 65 mM KCl–125 mM sucrose. General ATPase activity was detected by measuring the decrease in $A_{340}$ in a coupled enzyme assay at 30°C (19). Each sample (5 μl) was mixed with 100 μl of a reaction mixture containing 30 mM HEPES, 200 mM KCl, 4 mM $MgCl_2$, 50 μM EGTA, 1 mM phosphoenolpyruvate, 5 mM ATP, pyruvate kinase at 14 U/ml, lactate dehydrogenase at 20 U/ml, and 0.3 mM NADH, pH 7.6. Other enzymes were assayed as described previously (31, 38, 40) in 100-μl reaction mixtures. All assays, except for proton transport, were performed by using a PowerWave 340 plate reader (Bio-tek Instruments) at 30°C; PPase was assayed (by determining phosphate release) at the single wavelength of 360 nm. Protein was determined fluorometrically as described by Böhler et al. (2).

**Electron microscopy.** For observation of Percoll fraction 1, the fraction was washed in 0.25 M sucrose and a 5-μl sample was placed on a Formvar-coated copper or nickel grid, allowed to adsorb for 5 to 15 min at room temperature, blotted dry, and observed directly by electron microscopy (38). Whole trypomastigotes were applied to grids in a similar manner (37, 38). Energy-dispersive X-ray analysis was done at the Electron Microscopy Center, Southern Illinois University. Specimen grids were examined in a Hitachi H-7100FA transmission electron microscope at an accelerating voltage of 50 kV. Fine probe sizes were adjusted to cover the electron-dense granules (or a similar area of the background), and X-rays were collected for 100 s by utilizing a thin-window (Norvar) detector. Analysis was performed by using a Noran Voyager III analyzer with a standardless analysis identification program. Conventional electron microscopy (see Fig. 7) was done as previously described (37).

## RESULTS

**$PP_i$ drives proton transport in permeabilized procyclic trypomastigotes.** As reported previously (35, 42), when procyclic trypomastigotes were permeabilized with digitonin, some acridine orange was accumulated and retained in the absence of added energy sources (Fig. 1A). Once a steady state of acridine orange accumulation was reached, addition of 0.1 mM $PP_i$ led

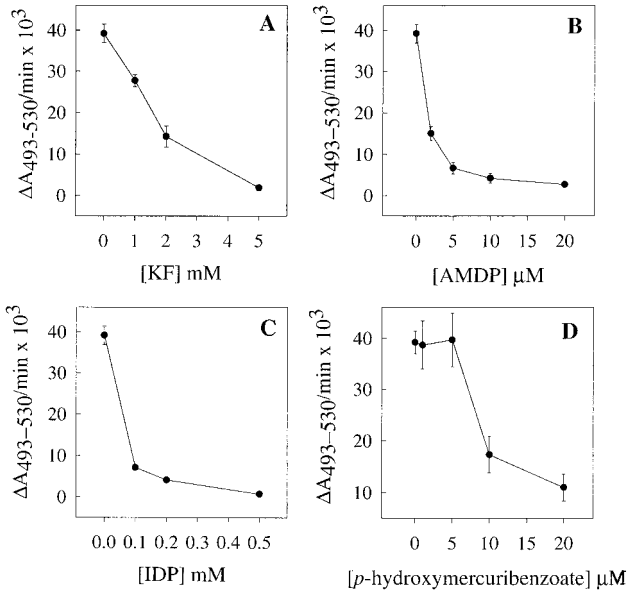


FIG. 2. Inhibition of V-H$^+$-PPase activity in permeabilized procyclic trypomastigotes by KF, IDP, AMDP, and *p*-hydroxymercuribenzoate. All assays were run in the standard buffer described in the legend to Fig. 1B. Procyclic trypomastigotes (0.1 mg of protein/ml) were incubated with inhibitors for 3 min, during permeabilization, prior to the addition of 0.1 mM $PP_i$. The results are expressed as $\Delta A_{493-530}$/min $\times 10^3$. Error bars indicate SEs of mean values of at least three separate experiments.

to further dye uptake (trace a). This indicated the establishment of a proton gradient (ΔpH) across the membrane of an intracellular compartment and increasing organelle acidity. This gradient collapsed completely after the addition of 1 μM nigericin or 20 mM $NH_4Cl$ (data not shown). Replacement of the KCl in the buffer with NaCl (trace c) or *N*-methylglucamine chloride (trace e) reduced the acidification rate. More KCl in the buffer slightly increased the amount of acridine orange accumulated (trace b), while more NaCl further decreased the acidification rate (trace d compared with trace c). Use of a buffer containing equimolar (65 mM) concentrations of NaCl and KCl resulted in slightly more acridine orange uptake (trace f) than in the presence of 130 mM KCl (trace b). These results indicate that the PPase was stimulated by $K^+$, similar to plant (33) and *T. cruzi* (38) V-H$^+$-PPases. This dependence differentiates V-H$^+$-PPases from known mitochondrial H$^+$-PPases, which do not require $K^+$ (25).

As occurs with plant vacuoles (27), the protonophore FCCP (Fig. 1B) or carbonyl cyanide *m*-chlorophenylhydrazone (data not shown) only partially dissipated $PP_i$-induced proton gradients. This suggested that there was a positive (inside) membrane potential of sufficient magnitude to drive partial proton efflux in the presence of the ionophores but that further proton release was inhibited by the relative impermeability of the vacuole membrane(s) to countercurrent cation, or concurrent anion, flow (required to maintain charge neutrality). A $PP_i$-dependent membrane potential was demonstrated in isolated acidocalcisomes (see below). Addition of valinomycin after FCCP completed the collapse of the proton gradient. Membranes become permeable to $K^+$ in the presence of valinomycin (a $K^+$ ionophore), and the action of the combination FCCP plus valinomycin resembled that of nigericin (a $K^+/H^+$ exchanger) (Fig. 1A). In agreement with this explanation, when the order of additions was reversed, valinomycin slightly increased acridine orange uptake and this was released after addition of FCCP (Fig. 1B).

In contrast to the results obtained with procyclic trypomastigotes (Fig. 1), no acridine orange uptake could be detected when permeabilized bloodstream trypomastigotes were used under similar conditions, even if the amount of protein used was increased 10-fold (data not shown). ATP, in contrast to $PP_i$, was able to induce acridine orange uptake by permeabilized bloodstream trypomastigotes (data not shown), in agreement with results previously reported (35, 42).

**Inhibition of the V-H$^+$-PPase activity of permeabilized procyclic trypomastigotes.** $PP_i$-induced acidification of the intracellular compartment of procyclic trypomastigotes was inhibited in a dose-dependent manner by KF (Fig. 2A), by the $PP_i$ analogs AMDP (Fig. 2B) and IDP (Fig. 2C), and by the thiol reagent *p*-hydroxymercuribenzoate (Fig. 2D). The effective concentrations of KF, AMDP, and IDP were similar to those that inhibit plant V-H$^+$-PPase activity (47, 50). The effects of different known H$^+$-ATPase inhibitors on $PP_i$-dependent acridine orange uptake by permeabilized trypomastigotes were also investigated. Sodium *o*-vanadate, a P-type H$^+$-ATPase inhibitor (15), and low concentrations of *N*,*N*′-dicyclohexylcarbodiimide, a general proton pump inhibitor (39), did not significantly affect this activity (Table 1). Bafilomycin $A_1$ and concanamycin A, two specific V-H$^+$-ATPase inhibitors, when used at nanomolar concentrations (13), were also ineffective (Table 1). The concentrations used here were the minimum amounts found previously to completely inhibit the V-H$^+$-ATPase activity of *T. cruzi* (36) (Table 1). 7-Chloro-4-nitrobenz-2-oxa-1,3-diazole, which is a more nonspecific V-H$^+$-ATPase inhibitor (15), was inhibitory (Table 1), and the mitochondrial H$^+$-ATPase inhibitor oligomycin (1 μM) and *N*-ethylmaleimide (100 μM) had no effect (data not shown).

**The V-H$^+$-PPase of permeabilized procyclic trypomastigotes has a low $K_m$ for $PP_i$ and a neutral pH optimum and is not dependent on the presence of a particular anion.** The dependence of the initial rate of acridine orange absorbance decrease upon the $PP_i$ concentration in permeabilized procyclic trypomastigotes is shown in Fig. 3A. The double-reciprocal plot of the data (inset) yields a straight line from which a $K_m$ of approximately 2 μM was calculated. Figure 3B shows the effect of medium pH on this reaction. Activity was optimal in the pH range of 7.0 to 7.5. Table 2 shows that the initial reaction rate was not significantly affected when $SO_4^-$, $NO_3^-$, $HCO_3^-$, $Cl^-$, or gluconate was used as the anion.

**Evidence for colocalization of V-H$^+$-PPase and V-H$^+$-ATPase activities in procyclic trypomastigotes and its relationship to H$^+$/Na$^+$ antiport activity.** Since the vacuolar H$^+$-ATPase and the H$^+$-translocating PPase colocalize in vacuoles

TABLE 1. Effects of ATPase inhibitors on $PP_i$-driven proton transport in permeabilized procyclic trypomastigotes of *T. brucei*[a]

| Inhibitor (concn [μM]) | $PP_i$-dependent H$^+$ transport ($\Delta A_{493-530}$/min $\times 10^3$) | % of control |
|---|---|---|
| None (control) | 39.2 ± 2.2 | 100 |
| Concanamycin A (0.005) | 34.3 ± 2.2 | 87 |
| Bafilomycin $A_1$ (0.040) | 38.3 ± 3.7 | 97 |
| Sodium *o*-vanadate (500) | 45.0 ± 1.8 | 114 |
| DCCD (50) | 35.3 ± 0.7 | 90 |
| NBD-Cl (10) | 25.8 ± 2.1 | 65 |

[a] Proton transport was assayed by using acridine orange, as described in Materials and Methods, in the standard buffer described in the legend to Fig. 1B. Inhibitors were added after 3 min of permeabilization, prior to the addition of 0.1 mM $PP_i$. The values are means ± SEs of three experiments.

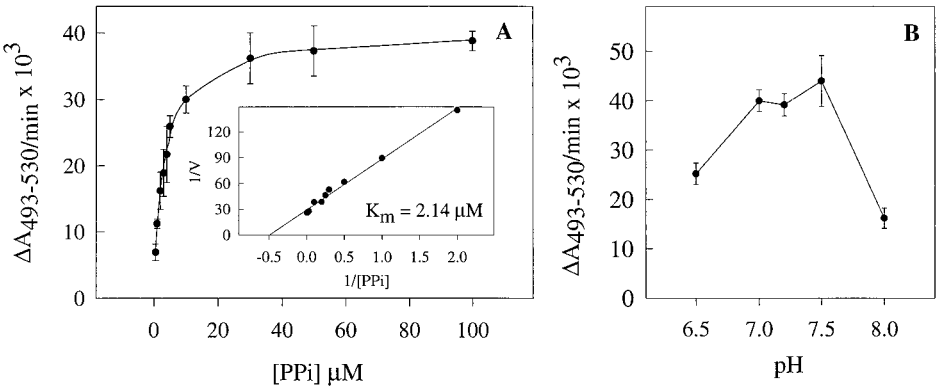


FIG. 3. Initial rate of $PP_i$-dependent proton uptake by permeabilized procyclic trypomastigotes as a function of substrate concentration (A) and medium pH (B). Experimental conditions were as described in the legend to Fig. 1B with different concentrations of $PP_i$ (A) or in the same buffer adjusted to different pH values (B). The inset (A) represents the linear transformation, by double-reciprocal plot, of the curve. The $K_m$ for $PP_i$ was calculated by using a computerized nonlinear regression program (Sigma Plot 1.0; Jandel Scientific) to analyze the data with the Michaelis-Menten equation. The results are indicated as $\Delta A_{493-530}$/min $\times$ $10^3$. Error bars indicate SEs of mean values of at least three separate experiments.

of higher plant cells (33), we investigated whether they also colocalize in *T. brucei*. We approached this first by measuring acridine orange uptake in permeabilized cells in the presence of different substrates.

Addition of ATP after a steady state of acridine orange accumulation was reached led to further uptake of acridine orange (Fig. 4A, trace a). $PP_i$ addition further stimulated acridine orange uptake, at a rate faster than that obtained with ATP but to an extent lower than that generated by $PP_i$ alone (Fig. 4A, trace b). When the order of additions was reversed, $PP_i$ caused fast accumulation of acridine orange but addition of ATP did not lead to further accumulation of the dye (Fig. 4A, trace b). This was not due to a deficiency of acridine orange in the medium, as addition of more of the dye did not have any effect (data not shown). In both cases, acridine orange was immediately released by addition of $NH_4Cl$. These results suggest that the ATP-driven and $PP_i$-driven proton pumps are located in the same compartment.

$Na^+$ ions added to digitonin-permeabilized *T. brucei* procyclic trypomastigotes were previously shown to reduce ATP-generated proton gradients, suggesting the operation of an $Na^+/H^+$ exchanger in these cells (43). Colocalization of the V-$H^+$-ATPase and the V-$H^+$-PPase in *T. brucei* procyclic trypomastigotes might therefore be demonstrated by comparing $Na^+$-dependent proton efflux from (nonmitochondrial) compartments previously acidified with either ATP or $PP_i$. *T. brucei* procyclics were permeabilized first in $Na^+$-free medium containing mitochondrial inhibitors, and either ATP or $PP_i$ was added. In agreement with previous results (43, 44), partial release of acridine orange, accumulated after ATP addition, could be induced by the addition of 40 mM NaCl (Fig. 5A, trace a). However, 40 mM KCl was ineffective (data not shown), indicating that the effect was not due to changes in osmotic pressure and that $Na^+$ was the active cation.

Initial experiments, in which acridine orange accumulation was driven by $PP_i$ instead of ATP, indicated that addition of either 40 mM NaCl (Fig. 5A, trace b), 40 mM KCl, or 40 mM choline chloride (data not shown) resulted not in acridine orange efflux but in slight acidification. However, we reasoned that ADP produced by hydrolysis of ATP could have stimulated the $Na^+/H^+$ exchanger. In agreement with this, addition of ADP after NaCl stimulated acridine orange release from the compartment previously acidified by either $PP_i$ (trace b) or ATP (trace a). ADP addition alone produced a slow acridine

TABLE 2. Effects of different potassium salts on $PP_i$-driven proton transport in permeabilized procyclic trypomastigotes of *T. brucei*[a]

| Potassium salt | $PP_i$-dependent $H^+$ transport ($\Delta A_{493-530/min \times 10^3}$) | % of control |
|---|---|---|
| KCl (control) | 39.2 ± 2.2 | 100 |
| Potassium gluconate | 38.8 ± 2.7 | 99 |
| $K_2SO_4$ | 48.7 ± 4.0 | 124 |
| $KNO_3$ | 35.4 ± 3.9 | 90 |
| $KHCO_3$ | 32.5 ± 3.9 | 90 |

[a] Proton transport was assayed by using acridine orange, as described in Materials and Methods, in the standard buffer described in the legend to Fig. 1B except that KCl was replaced with the other salts. The values are means ± SEs of three experiments.

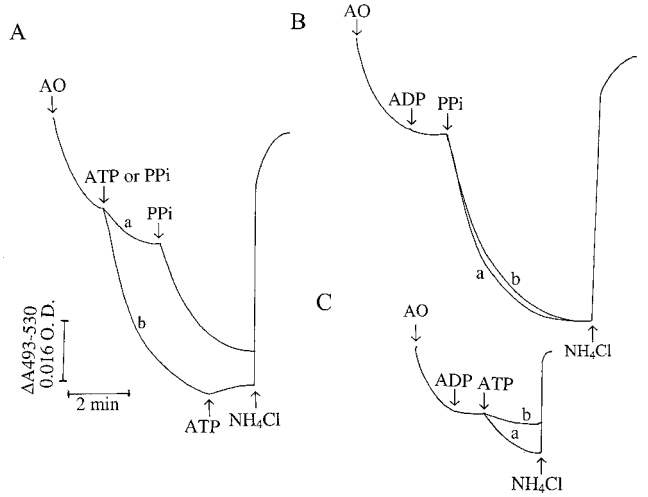


FIG. 4. ATP- and $PP_i$-dependent proton uptake by permeabilized procyclic trypomastigotes. Experimental conditions were as described in the legend to Fig. 1B. (A) ATP (1 mM) was added before (trace a) or after (trace b) addition of $PP_i$. (B) Procyclic trypomastigotes (0.1 mg of protein/ml) were incubated in the absence (trace a) or presence (trace b) of 1 mM ADP, which was added before addition of 0.1 mM $PP_i$. (C) Same as panel B, except that $PP_i$ was replaced with 1 mM ATP. Acridine orange (AO; 3 μM), ADP (1 mM), ATP (1 mM), $PP_i$ (0.1 mM), or $NH_4Cl$ (10 mM) was added where indicated by the arrows. O.D., optical density.

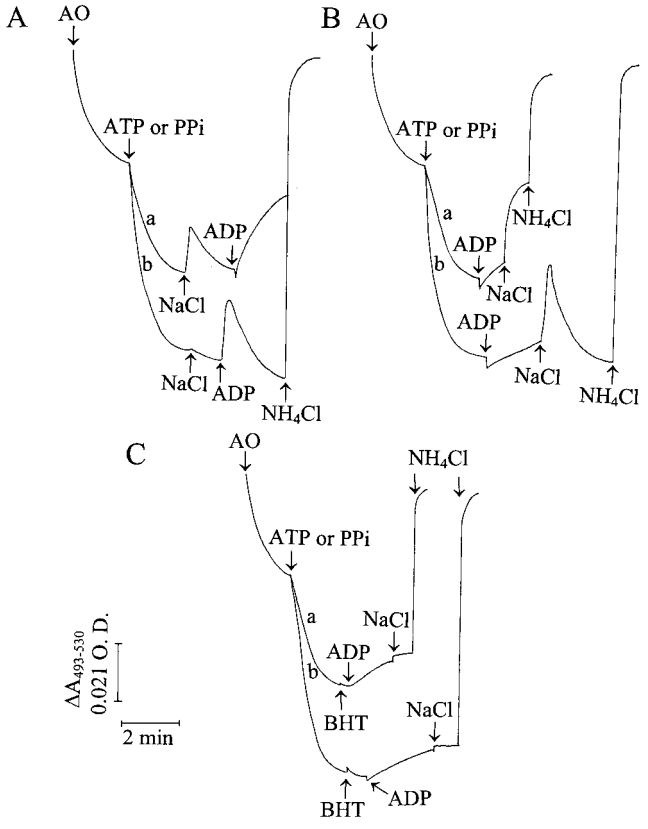


FIG. 5. Effects of NaCl and ADP on ATP- and $PP_i$-dependent proton uptake by permeabilized procyclic trypomastigotes. Procyclic trypomastigotes (0.1 mg of protein/ml) were incubated in a reaction mixture containing 65 mM KCl, 125 mM sucrose, 2 mM $MgCl_2$, 250 μM EGTA, 2 mM $KH_2PO_4$, 10 mM HEPES (pH 7.2), 16 μM digitonin, antimycin A at 1 μg/ml, and oligomycin at 2 μg/ml. In all of the panels, trace a represents proton uptake by 1 mM ATP and trace b represents proton uptake by 0.1 mM $PP_i$. (A) NaCl (40 mM) was added before addition of 1 mM ADP. (B) ADP (1 mM) was added prior to the addition of 40 mM NaCl. (C) BHT (20 μM) was added prior to the addition of 1 mM ADP and 40 mM NaCl. Acridine orange (AO; 3 μM), ATP (1 mM), $PP_i$ (0.1 mM), ADP (1 mM), NaCl (40 mM), BHT (20 μM), and $NH_4Cl$ (20 mM) were added where indicated by the arrows. O.D., optical density.

orange release which was greatly stimulated by addition of NaCl (Fig. 5B). This proton release by ADP appeared to be due to a direct effect of the nucleotide on the $Na^+/H^+$ exchanger and not to an inhibitory effect on the V-$H^+$-PPase, since the rapid release of protons was detected only when both ADP and $Na^+$ were present. Addition of ADP before $PP_i$ did not cause any inhibition of proton transport (Fig. 4B, trace b), whereas it did inhibit ATP-dependent $H^+$ uptake (Fig. 4C, trace b).

To confirm the mode of action of ADP, we tested its effect in the presence of 3,5-dibutyl-4-hydroxytoluene (BHT), an antioxidant that has been shown to inhibit the $Na^+/H^+$ exchanger in *T. brucei* (44). Addition of BHT before ADP did not interfere with the slow acridine orange release promoted by ADP (Fig. 5C). However, the fast release of protons caused by NaCl was suppressed, suggesting that ADP directly affected the $Na^+/H^+$ exchanger.

**Detection of $PP_i$ activity in both procyclic and bloodstream trypomastigotes and effects of buffer composition.** $PP_i$ was also assayed in membrane preparations of *T. brucei* by inorganic-phosphate detection by using PNP and MESG as cosubstrates with phosphate (48). In contrast to the results obtained from $H^+$-pumping assays of permeabilized preparations, this activity was detected in both procyclic and bloodstream trypomastigotes (Table 3). Total PPase activity in membrane preparations of procyclic and bloodstream trypomastigotes was inhibited by 20 μM AMDP by 75% ± 4% and 58% ± 4% (average ± standard error [SE] of five and eight experiments, respectively). The lower inhibition by AMDP of $PP_i$ hydrolysis compared to $PP_i$-dependent $H^+$ transport (Fig. 2) could indicate the presence of other non-$H^+$-translocating or AMDP-sensitive PPases or nonspecific phosphatase activities in these preparations. The effects of monovalent cations on AMDP-inhibitable activity in procyclic trypomastigotes were, in general, similar to those found in the acridine orange assay, and no activity was detectable if KCl in the medium was replaced with *N*-methylglucamine chloride. When membranes from bloodstream trypomastigotes were used, the activity decreased as the KCl concentration increased (Table 3). Specific activities in membrane preparations of procyclic and bloodstream trypomastigotes were 0.116 ± 0.048 and 0.038 ± 0.006 μmol of $PP_i$ consumed/min · mg of protein (means ± SE of results from five and eight separate experiments, respectively).

TABLE 3. Effect of buffer composition on PPase activity in *T. brucei* procyclic and bloodstream trypomastigotes[a]

| Buffer concn(s) | PPase activity (% of control) | |
|---|---|---|
| | Procyclic trypomastigotes | Bloodstream trypomastigotes |
| 65 mM KCl, 125 mM sucrose | 100 | 100 |
| 130 mM KCl | 114.7 ± 16.3 | 69.3 ± 12.6 |
| 65 mM NaCl, 125 mM sucrose | 11.6 ± 2.6 | 11.4 ± 1.7 |
| 130 mM NaCl | 28.3 ± 2.1 | 37.4 ± 6.9 |
| 65 mM NMG, 125 mM sucrose | 0 | 0 |
| 65 mM KCl, 65 mM NaCl | 69.6 ± 10.3 | 64.6 ± 8.9 |

[a] PPase activity was assayed by the PNP-MESG method as described in Materials and Methods. Rates are relative percentages compared to that obtained with the 65 mM KCl–125 mM sucrose buffer. In all cases, AMDP (20 μM)-sensitive rates are indicated. All buffers contained, in addition, 2 mM $MgSO_4$, 10 mM HEPES, and 50 μM EGTA and were adjusted to pH 7.2 with KOH, NaOH, or Tris base for the KCl, NaCl, and *N*-methylglucamine chloride (NMG) buffers, respectively. The values are means ± SEs of three experiments. Control activities for procyclic and bloodstream trypomastigotes were 0.116 ± 0.048 and 0.038 ± 0.006 μmol/min mg of protein, respectively.

**The V-$H^+$-PPase is located in acidocalcisomes in procyclic and bloodstream trypomastigotes.** To further analyze the subcellular location of the V-$H^+$-PPase, extracts of bloodstream and procyclic trypomastigotes were separated in Percoll gradients (Fig. 6). This method has been used before for the separation of organelles of unusually high density such as the rhoptries of *T. gondii* (21). The V-$H^+$-PPase could be detected by proton uptake in fractions from both bloodstream and procyclic forms, as well as by phosphate release, and as assayed by both methods, was concentrated toward the bottom (dense end) of the gradient (fraction 1), with another peak in the middle of the gradient (fraction 9), as found with *T. cruzi* (38). Electron microscopic examination of fractions 8 to 11 showed that they contained mitochondria, membranes, and ghosts, some of which had trapped organelles, including electron-dense vacuoles (data not shown). Digitonin treatment reduced $H^+$-PPase activity in fractions from bloodstream forms by 35 to 50% (in all portions of the gradient where activity was detectable) but had no consistent effect on $H^+$-PPase activity in fractions from procyclics, thus explaining why this proton-pumping activity could not be detected in digitonin-permeabilized bloodstream forms. Markers for other compartments and general ATPase activity (ATP hydrolysis) all peaked further up the gradient, in the region of fractions 6 to 11. No proton-

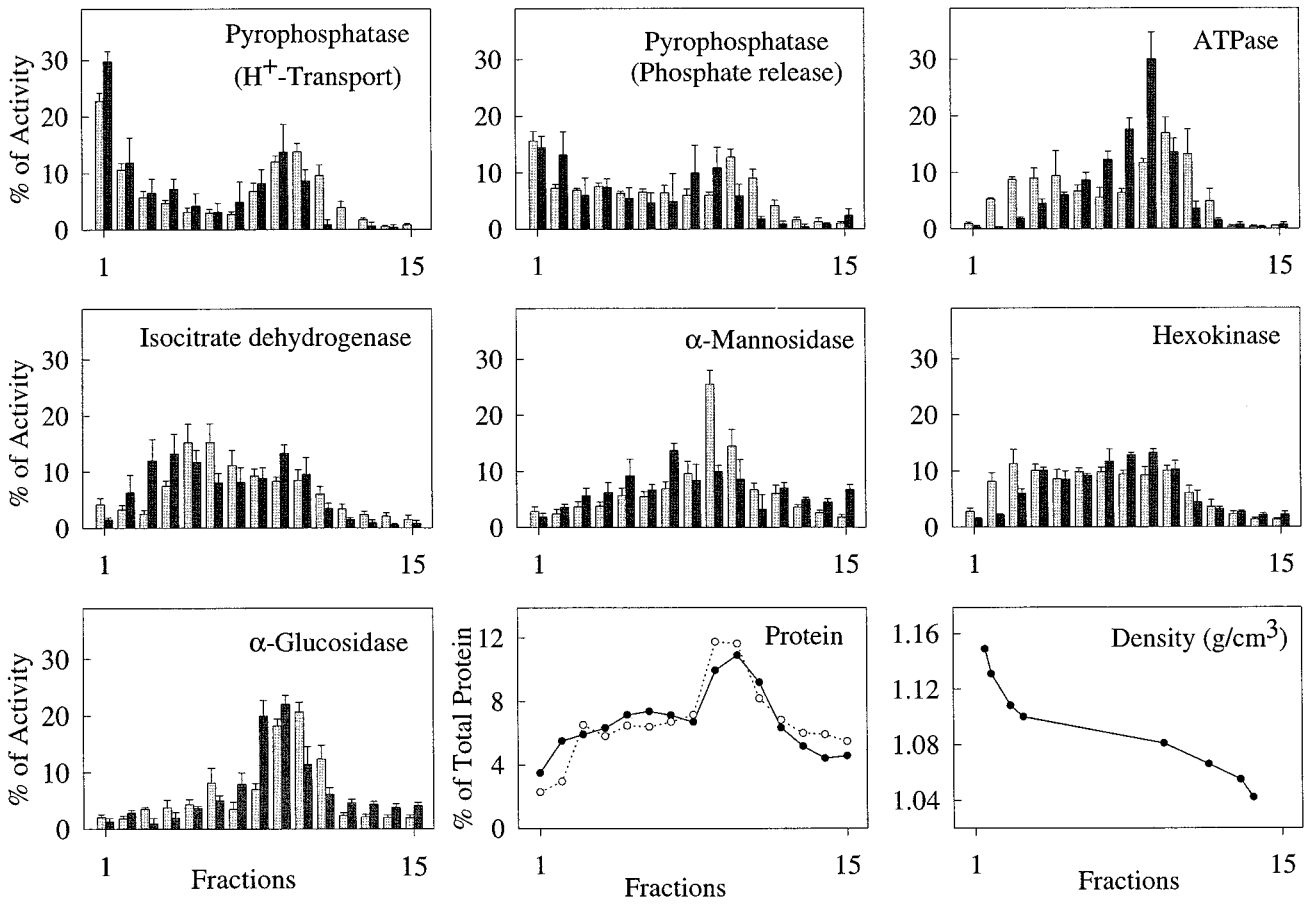


FIG. 6. Distribution of PPase activity from procyclic and bloodstream trypomastigotes on Percoll gradients. PPase is concentrated in a distinct dense fraction. V-$H^+$-PPase activity, measured by proton uptake or phosphate release, was compared with the distribution of ATPase activity and the established organelle markers isocitrate dehydrogenase (mitochondria), α-mannosidase (lysosome), hexokinase (glycosome), and α-glucosidase (plasma membrane). Charts show mean activity ± SE (as a percentage of the total recovered activity) from three to seven independent experiments. Light gray bars represent procyclics, and dark gray bars represent bloodstream trypomastigotes. Density was measured in a single experiment by using Percoll density marker beads. Protein distribution in the different fractions of procyclic and bloodstream trypomastigotes is indicated by closed and open circles, respectively.

pumping ATPase activity could be detected in any of the fractions (data not shown). The average amount of each organelle marker found in fraction 1 was under 5% of the total recovered activity of that marker, compared with 22 to 30% ($H^+$ transport) or 16 to 18% ($P_i$ release) of $H^+$-PPase activity, and since most of the recovered protein was in fractions 8 to 11 (Fig. 6), this method allowed significant purification of the $H^+$-PPase activity.

Examination of fraction 1 by transmission electron microscopy with conventional fixation, dehydration, and staining procedures showed round organelles of various sizes, up to 200 μm in diameter, containing an electron-dense region (Fig. 7B). These were similar to organelles found in sections of procyclic (Fig. 7A) or bloodstream trypomastigotes (not shown) and described previously as inclusion vacuoles (45) or polyphosphate bodies (7).

Transmission electron microscopy without fixation and staining of fraction 1 from procyclic (Fig. 8A) or bloodstream (Fig. 8D) trypomastigotes showed homogeneously electron-dense organelles (of various sizes, like those detected in fixed preparations [Fig. 7]). These organelles were also observed in whole procyclic (Fig. 9A) or bloodstream (Fig. 9B) trypomastigotes prepared in a similar manner and were similar to those previously identified as acidocalcisomes in *T. cruzi* (37, 38). When they were submitted to the electron beam, the organelles showed changes in their internal structure leading to the appearance of a sponge-like structure (Fig. 8D, inset) as occurs with *T. cruzi* acidocalcisomes (24). To confirm this identification, X-ray microanalysis was performed on the fraction 1 preparations (Fig. 8B and E). The spectra shown were the ones that yielded the most counts in 100 s (out of 10 spectra obtained for each stage), but all other spectra taken from dense organelles were qualitatively similar: phosphorus counts were about twofold greater than calcium counts, which were about twofold greater than magnesium counts. Zinc was present in some spectra (not shown). We also performed X-ray microanalysis of acidocalcisomes in whole parasites as described in Materials and Methods. Because of the small size of these parasites, the electron-dense acidocalcisomes could be easily identified. Acidocalcisomes were submitted to X-rays after adjustment of the fine probe size to cover their area. Spectra obtained from acidocalcisomes in whole trypomastigotes (Fig. 9C and D) were similar to those taken from the isolated organelles (Fig. 8B and E), except that more sodium was detected in whole procyclic trypomastigotes and more magnesium was detected in whole bloodstream trypomastigotes. Peaks for calcium, phosphorus, magnesium, and zinc were not present in spectra taken from the fraction 1 sample back-

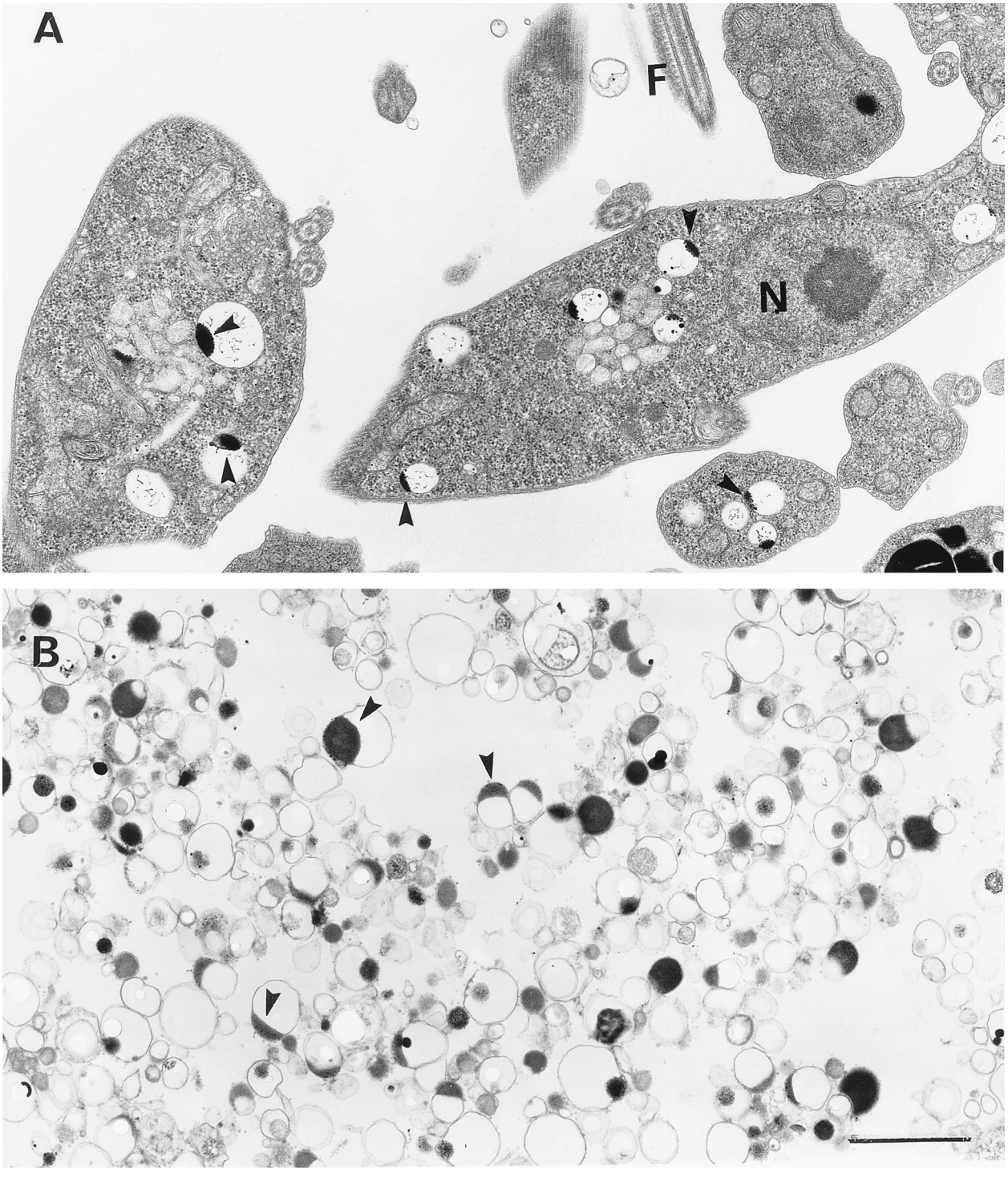


FIG. 7. Transmission electron microscopy of procyclic trypomastigotes (A) and isolated dense acidocalcisomes (B) from the same cells. The preparations were fixed and processed for conventional electron microscopy. Arrowheads in panels A and B show clear vacuoles with electron-dense inclusions closely apposed to the bounding membrane along one side. N, nucleus; F, flagellum. Bar (for A and B), 1 μm.

ground (Fig. 8C and F) or in the background from the whole-cell preparations (data not shown). Peaks for copper arise from the grid, and peaks for silicon arise from traces of Percoll in the specimens.

**Functional aspects of isolated acidocalcisomes—membrane potential and presence of $Na^+/H^+$ antiport.** The generation of a $PP_i$-dependent membrane potential ($\Delta\Psi$) was demonstrated in acidocalcisomes isolated from procyclics by the shift in Oxonol VI absorbance (Fig. 10A, trace a). This membrane potential was dissipated by FCCP (dashed line), and its generation was prevented by AMDP (trace b).

$Na^+/H^+$ antiport activity was detectable in isolated procyclic

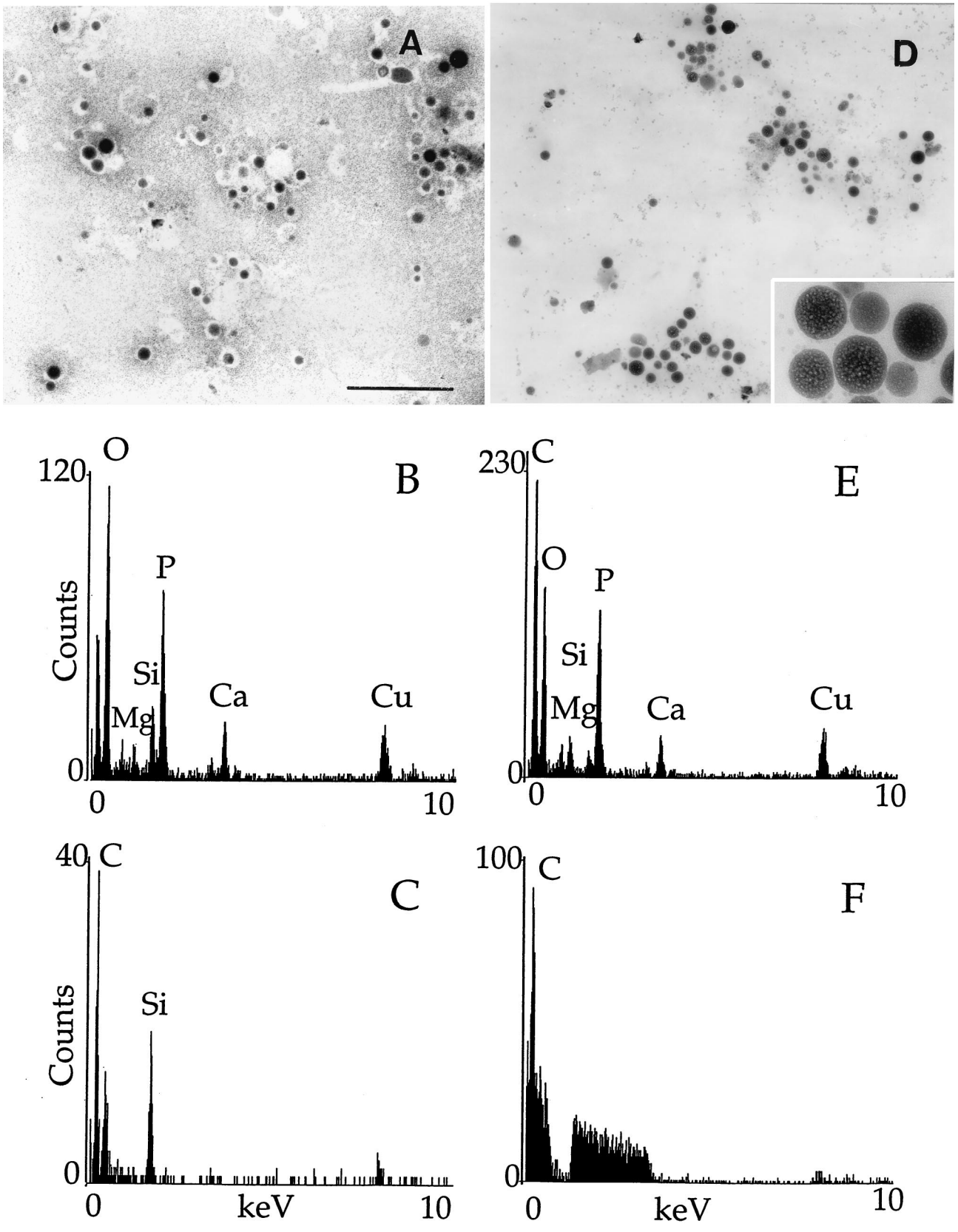


FIG. 8. Electron microscopy and X-ray microanalysis of the dense fraction containing PPase activity. Panels: A to C, procyclic trypomastigotes; D to F, bloodstream trypomastigotes. (A and D) Direct observation of Percoll fraction 1. Scale bar (for A and D), 2 μm. The inset in panel D shows a fourfold-higher magnification of the sponge-like structure of the acidocalcisomes after submission to the electron beam. (B and E) X-ray microanalysis spectra of dense organelles in fraction 1. (C and F) X-ray microanalysis spectra of the background to fraction 1 preparations.

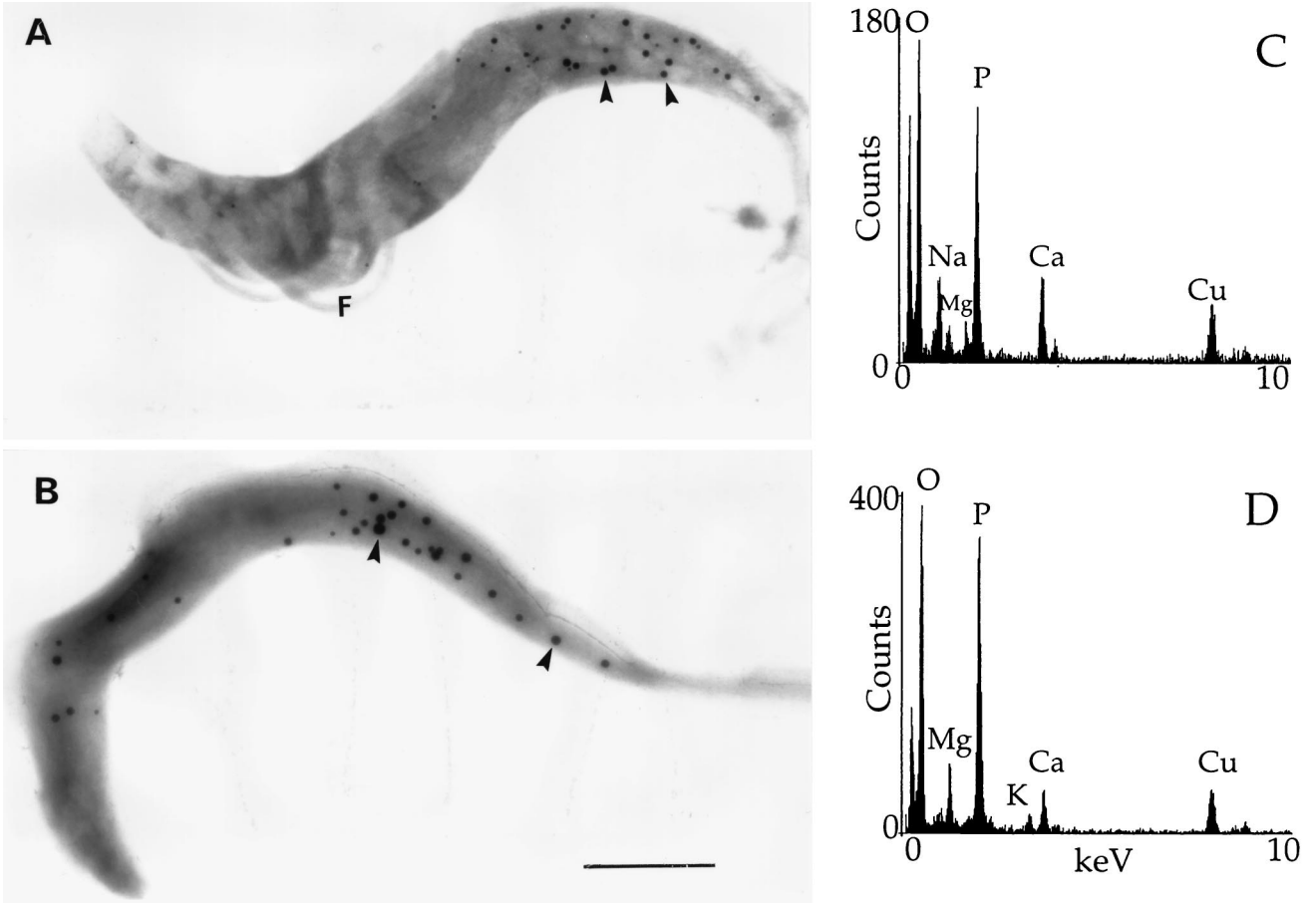


FIG. 9. Transmission electron microscopy of whole procyclic (A) and bloodstream (B) trypomastigotes treated similarly to the fractions in Fig. 8. Scale bar (for A and B), 2 μm. X-ray microanalysis spectra of dense organelles in whole procyclic (C) and bloodstream (D) trypomastigotes. The arrowheads indicate acidocalcisomes.

acidocalcisomes, as shown in Fig. 10B. Following organelle acidification by $PP_i$, addition of either NaCl or KCl at 40 mM produced equivalent further increases in acidification. This may be attributable to the addition of more chloride, which could act as a counterion to $H^+$, reduce the membrane potential, and allow the generation of a greater proton gradient. This is in agreement with the experiment whose results are shown in Fig. 1, traces a, b, and f, in which the presence of more chloride increased the extent of acidification after $PP_i$ treatment of permeabilized procyclics, and with similar results obtained with permeabilized procyclics (Fig. 5A, trace b). ADP addition after KCl treatment had no effect (Fig. 10B, dashed line). However, ADP addition after NaCl treatment caused a transient release of protons, indicating that the ADP-stimulated $Na^+/H^+$ antiport was present in this fraction.

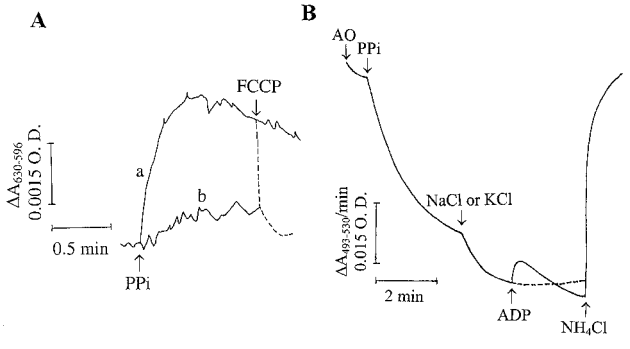


FIG. 10. Generation of a membrane potential by $PP_i$ and $PP_i$-dependent proton uptake in isolated acidocalcisomes from procyclic trypomastigotes. (A) Membrane potential was measured as described in Materials and Methods by using Oxonol VI. The dense fraction obtained by cell fractionation (fraction 1; Fig. 6) was incubated in the standard buffer described in the legend to Fig. 1B containing, in addition, 1 μM Oxonol VI. The membrane potential was measured in the absence (trace a) and presence (trace b) of 20 μM AMDP. $PP_i$ (0.1 mM) and FCCP (1 μM) were added where indicated by the arrows. (B) Fraction 1 was added to the standard buffer described in the legend to Fig. 1B without digitonin. Acridine orange (AO; 3 μM), $PP_i$ (0.1 mM), NaCl or KCl (40 mM), and $NH_4Cl$ were added where indicated by the arrows. Only one trace is shown for NaCl and KCl because the traces were superimposable. O.D., optical density.

## DISCUSSION

In this study, we have identified and characterized an $H^+$-translocating PPase in permeabilized procyclic trypomastigotes of *T. brucei*. Like ATP-dependent proton transport (35, 42–44), acridine orange uptake in the presence of $PP_i$ was reversed by the $K^+/H^+$ exchanger, nigericin, or by alkalinization of the acidic compartment with $NH_4Cl$.

Several observations suggest that the $H^+$-PPase activity is distinct from that of known $H^+$-ATPases. First, as occurs with plant vacuolar PPases (33), $PP_i$-driven proton transport was blocked by KF and by the $PP_i$ analogs IDP and AMDP but was stimulated by potassium ions and was only partially reversed by protonophores. Second, the $H^+$-PPase was insensitive to bafilomycin $A_1$ and concanamycin A, two specific inhibitors of V-$H^+$-ATPases (13). Third, unlike P-type $H^+$-ATPases (15)

the $H^+$-PPase was insensitive to sodium *o*-vanadate. Fourth, like the plant vacuolar PPase, the proton-translocating activity required a permeant anion and was not inhibited by $NO_3^-$, as are many V-$H^+$-ATPases (15).

The presence of a PPase activity in the cytosolic, lysosomal, and flagellar-pocket fractions of bloodstream trypomastigotes of *T. brucei* was reported recently (29). However, these assays were performed with 0.1 M Tris/HCl buffer, pH 8.4, supplemented with 5 mM magnesium acetate (cytosolic fraction) or with 0.1 M sodium acetate, pH 3.9, without magnesium (lysosomal and flagellar-pocket fractions) and with 2 mM tetasodium $PP_i$ as the substrate. The lack of potassium ions and the suboptimal pH conditions (cf. Fig. 1A and 3B and Table 3) meant that the $H^+$-PPase was probably not detected in these experiments, and the possibility that general phosphatases could account for the activities was not ruled out.

We investigated the relationship of V-$H^+$-PPase to V-$H^+$-ATPase activity in *T. brucei*. In plants, these two activities are located in the same membrane—the vacuolar tonoplast (33). We made sequential additions of ATP and $PP_i$ to permeabilized procyclic trypomastigotes (Fig. 4) and measured the effects of ADP and NaCl on acridine orange release from acidic compartments (Fig. 5). The lack of additivity of acidification induced by ATP or $PP_i$ (Fig. 4A) and the essentially identical effects of NaCl on acridine orange release following the addition of either proton pump substrate (allowing for ADP inhibition of the $H^+$-ATPase; Fig. 4C and 5) suggest that both $H^+$ pumps are present in the same vacuole. Although no proton-pumping ATPase activity could be detected in isolated acidocalcisomes, this could be attributed to the loss of essential subunits of the vacuolar $H^+$-ATPase during the fractionation procedure as occurs during the purification of *Dictyostelium discoideum* endosomes (32). Unfortunately, we could not confirm the localization of the V-$H^+$-ATPase by using antibodies because no specific antibodies against integral membrane subunits of the *T. brucei* V-$H^+$-ATPase are available and none of the subunits have been purified. Heterologous antibodies used previously with *T. cruzi* (24) were not useful against the *T. brucei* enzyme (data not shown).

Proton-translocating PPase activity was undetectable in bloodstream trypomastigotes in permeabilization experiments. This was probably due to low activity compared to procyclics plus digitonin rendering internal membranes of bloodstream forms leaky to protons. Previously, we were able to detect $Ca^{2+}$ uptake driven by ATP in acidocalcisomes of digitonin-treated bloodstream forms, but only intermittently (35). Other data indicate that internal membranes, as well as plasma membranes, of trypanosomatids can be permeabilized by digitonin, depending upon the concentration used and the incubation time (6). Digitonin permeabilizes membranes by a specific interaction with 3β-hydroxysterols (11). Although procyclics can synthesize sterols (8), bloodstream forms are dependent upon uptake of host lipoprotein, which has to be broken down by proteases in endosomes or lysosomes to release cholesterol (9). This likely results in a different distribution of sterols in cellular membranes in these forms. The greater susceptibility of bloodstream forms to digitonin was confirmed by treatment of membrane fractions isolated on Percoll gradients. Digitonin had no consistent effect on proton uptake by procyclic fractions but reduced the rate of proton uptake by fractions from bloodstream forms by an average of 40%. Here, the finding of $H^+$-ATPase (but not $H^+$-PPase) activity in permeabilized bloodstream forms suggests that this pump is also located in vacuoles, which are more resistant to digitonin than are acidocalcisomes. Our results obtained with *T. cruzi* (37, 38) indicate that acidocalcisomes are distinct from lysosomes, which presumably possess V-$H^+$-ATPase activity.

V-$H^+$-PPase activity was used as a marker for the purification and characterization, by X-ray microanalysis, of acidocalcisomes from both procyclic and bloodstream stages of *T. brucei* (Fig. 6 to 8). These results, together with those of our previous work with other trypanosomatids (34, 37, 38), demonstrate that the acidocalcisomes correspond to the inclusion vacuoles described by Vickerman and Tetley (45) in *T. cyclops* and to electron-dense vacuoles of other trypanosomatids (14, 20, 49). Such vacuoles were shown to contain large amounts of phosphorus, calcium, magnesium, sodium, and in some cases (14, 20, 45), zinc, as examined by X-ray microanalysis of intact (14, 20, 49) or cryosectioned (20) cells. These inclusion vacuoles, also termed polyphosphate bodies, are not accessible to horseradish peroxidase labeling via endocytosis, indicating that they do not belong to the endocytic apparatus (7). Similar results were obtained by using gold-transferrin to label the endosomes of *T. cruzi* (37). In this study, we also measured ATPase activity in fractions of the Percoll gradients used to purify the acidocalcisomes and found that the acidocalcisome-containing fraction had negligible ATPase activity. However, this does not rule out the presence of the V-$H^+$-ATPase in this fraction, as no proton-pumping ATPase activity could be detected in any *T. brucei* fraction, possibly due to the loss of some essential subunits during the fractionation procedure (as occurs during the purification of endosomes from *D. discoideum* [32]), or else because of enzyme oxidation (17).

Examination by electron microscopy of fractions 8 to 11 showed that they contained other organelles and ghosts, some of which had trapped acidocalcisomes. This explains, at least in part, the detection of V-$H^+$-PPase activity in these fractions. The material loaded onto the Percoll gradient had been clarified following lysis by centrifugation at only $500 \times g$ for 10 min (38). This ensured the maximum yield of acidocalcisomes in the bottom fraction but also failed to remove all of the cell ghosts from the lysate. In *T. cruzi*, the V-$H^+$-PPase has also been localized to the plasma membrane, as examined by immunofluorescence and immunoelectron microscopy using antibodies against peptide sequences present in the plant enzyme (38). However, these antibodies do not cross-react specifically with the *T. brucei* enzyme (data not shown) and we were unable to confirm a plasma membrane localization.

We were able to link the acidocalcisome, as detected in permeabilized cells, with the purified organelle by assaying for ADP-stimulated $Na^+/H^+$ exchange activity in the latter (Fig. 10B). ADP caused proton release in the presence of $Na^+$, but not when only $K^+$ was present, similar to the results obtained with permeabilized cells (Fig. 5). Figure 5A, trace b, shows that addition of NaCl slightly increased acidification in permeabilized cells, and only after addition of ADP was acridine orange released. Similar results were obtained with isolated acidocalcisomes (Fig. 10B). In the absence of ADP, KCl had the same effect as NaCl, which indicates that the increased acidification observed was due to the $Cl^-$ added and not to the cation added. These results imply that the acidocalcisome detected under both circumstances is the same organelle. In addition, the isolated organelles possess the two characteristics that we used to define the acidocalcisomes (42): they are acidic, as demonstrated by the $PP_i$-dependent proton transport (Fig. 10), and they contain large amounts of calcium, as detected by X-ray microanalysis (Fig. 8).

For the first time, we have shown that purified acidocalcisomes are able to generate a $PP_i$-dependent membrane potential (Fig. 10A). In plants, V-$H^+$-PPases catalyze inward electrogenic $H^+$ translocation from the cytosol to the vacuole

lumen to establish an inside-acid pH difference ($\Delta pH$) and an inside-positive electrical potential difference ($\Delta\Psi H^+$) which is employed to energize a wide range of secondary, $\Delta\Psi$- and/or $\Delta pH$-coupled, transport processes (33).

In conclusion, our results further indicate that acidocalcisomes are novel organelles with no counterpart in mammalian cells. Analysis of their role in parasite survival and pathogenesis is likely to lead to the discovery of novel targets for antitrypanosomatid chemotherapy.

## ACKNOWLEDGMENTS

We thank Philip A. Rea for the gift of AMDP, Nicole VanderHeyden and Wen Yan for help with the preparation of bloodstream trypomastigotes, and Linda Brown and Elizabeth Ujhelyi for technical assistance.

This work was supported by a grant from the UNDP/World Bank/World Health Organization Special Programme for Research and Training in Tropical Diseases to R.D. C.O.R. was a fellow of the Conselho Nacional de Desenvolvimento Científico e Tecnológico (CNPq), Brazil.

## REFERENCES

1. **Balscheffsky, M., S. Nadanaciva, and A. Schultz.** 1998. A pyrophosphatase synthase gene: molecular cloning and sequencing of the cDNA encoding the inorganic pyrophosphate synthase from *Rhodospirillum rubrum*. Biochim. Biophys. Acta **1364:**301–306.
2. **Böhler, P., S. Stein, W. Dairman, and S. Udenfriend.** 1973. Fluorometric assay of proteins in the nanogram range. Arch. Biochem. Biophys. **155:**213–220.
3. **Bowman, B. J., and E. J. Bowman.** 1986. $H^+$-ATPases from mitochondria, plasma membranes, and vacuoles of fungal cells. J. Membr. Biol. **94:**83–97.
4. **Brightman, A. O., P. Navas, N. M. Minnifield, and D. J. Morré.** 1992. Pyrophosphate-induced acidification of trans cisternal elements of rat liver Golgi apparatus. Biochim. Biophys. Acta Bio-Membr. **1104:**188–194.
5. **Brun, R., and M. Schönenberg.** 1979. Cultivation and in vitro cloning of procyclic culture forms of *Trypanosoma brucei* in a semi-defined medium. Acta Trop. **36:**289–292.
6. **Cazzulo, J. J., E. Valle, R. Docampo, and J. J. B. Cannata.** 1980. Intracellular distribution of $CO_2$ fixing enzymes in *Trypanosoma cruzi* and *Crithidia fasciculata*. J. Gen. Microbiol. **117:**271–274.
7. **Coppens, I., P. Baudhin, F. R. Opperdoes, and P. J. Courtoy.** 1993. Role of acidic compartments in *Trypanosoma brucei*, with special reference to low-density lipoprotein processing. Mol. Biochem. Parasitol. **58:**223–232.
8. **Coppens, I., and P. J. Courtoy.** 1995. Exogenous and endogenous sources of sterols in the culture-adapted procyclic trypomastigotes of *Trypanosoma brucei*. Mol. Biochem. Parasitol. **73:**179–188.
9. **Coppens, I., T. Levade, and P. J. Courtoy.** 1995. Host plasma low density lipoprotein particles as an essential source of lipids for the bloodstream forms of *Trypanosoma brucei*. J. Biol. Chem. **270:**5736–5741.
10. **Cross, G. A. M.** 1975. Identification, purification and properties of clone-specific glycoprotein antigens constituting the surface coat of *Trypanosoma brucei*. Parasitology **71:**393–417.
11. **Diaz, R., and P. D. Stahl.** 1989. Digitonin permeabilization procedures for the study of endosome acidification and function. Methods Cell Biol. **31:**25–43.
12. **Docampo, R., D. A. Scott, A. E. Vercesi, and S. N. J. Moreno.** 1995. Intracellular $Ca^{2+}$ storage in acidocalcisomes of *Trypanosoma cruzi*. Biochem. J. **310:**1005–1012.
13. **Dröse, S., and K. Altendorf.** 1997. Bafilomycins and concanamycins as inhibitors of V-ATPases and P-ATPases. J. Exp. Biol. **200:**1–8.
14. **Dvorak, J. A., J. C. Engel, R. D. Leapman, C. R. Swyt, and P. A. Pella.** 1988. *Trypanosoma cruzi*: elemental composition heterogeneity of cloned stocks. Mol. Biochem. Parasitol. **31:**19–26.
15. **Finbow, M., and M. A. Harrison.** 1997. The vacuolar $H^+$-ATPase: a universal proton pump of eukaryotes. Biochem. J. **324:**697–712.
16. **Forgac, M.** 1998. Structure, function and regulation of the vacuolar ($H^+$)-ATPases. FEBS Lett. **440:**258–263.
17. **Harvey, W. R., and H. Wieczorek.** 1997. Animal plasma membrane energization by chemiosmotic $H^+$ V-ATPases. J. Exp. Biol. **200:**203–216.
18. **Ikeda, M., M. D. Rahman, C. Moritani, K. Umami, Y. Tanimura, R. Akagi, Y. Tanaka, M. Maeshima, and Y. Watanabe.** 1999. A vacuolar $H^+$-pyrophosphatase in *Acetabularia acetabulum*: molecular cloning and comparison with higher plants and a bacterium. J. Exp. Bot. **50:**139–140.
19. **Jenkins, W. T.** 1991. The pyruvate kinase-coupled assay for ATPases, a critical analysis. Anal. Biochem. **194:**136–139.
20. **LeFurgey, A., P. Ingram, and J. J. Blum.** 1990. Elemental composition of polyphosphate-containing vacuoles and cytoplasm of *Leishmania major*. Mol. Biochem. Parasitol. **40:**77–86.
21. **Leriche, M. A., and J. F. Dubremetz.** 1991. Characterization of the protein content of rhoptries and dense granules of *Toxoplasma gondii* tachyzoites by subcellular fractionation and monoclonal antibodies. Mol. Biochem. Parasitol. **45:**249–260.
22. **Lichko, L., and L. Okorokov.** 1991. Purification and some properties of membrane bound and soluble pyrophosphatase of yeast vacuoles. Yeast **7:**805–812.
23. **Lu, H.-G., L. Zhong, K. P. Chang, and R. Docampo.** 1997. Intracellular $Ca^{2+}$ pool content and signaling, and expression of a calcium pump are linked to virulence in *Leishmania mexicana amazonensis*. J. Biol. Chem. **272:**9464–9473.
24. **Lu, H.-G., L. Zhong, W. de Souza, M. Benchimol, S. N. J. Moreno, and R. Docampo.** 1998. $Ca^{2+}$ content and expression of an acidocalcisomal calcium pump are elevated in intracellular forms of *Trypanosoma cruzi*. Mol. Cell. Biol. **18:**2309–2323.
25. **Lundin, M., S. W. Deopujari, L. Lichko, L. Pereira da Silva, and H. Baltscheffsky.** 1992. Characterization of a mitochondrial inorganic pyrophosphatase in *Saccharomyces cerevisiae*. Biochim. Biophys. Acta **1098:**217–223.
26. **Macri, F., and A. Vianello.** 1987. ADP- or pyrophosphate-dependent proton pumping of pea tonoplast-enriched vesicles. FEBS Lett. **215:**47–52.
27. **Macri, F., M. Zancani, E. Petrussa, P. Dell'Antone, and A. Vianello.** 1995. Pyrophosphate and $H^+$-pyrophosphatase maintain the vacuolar proton gradient in metabolic inhibitor-treated *Acer pseudoplatanus* cells. Biochim. Biophys. Acta **1229:**323–328.
28. **Mellman, I., R. Fuchs, and A. Helenius.** 1986. Acidification of the endocytic and exocytic pathways. Annu. Rev. Biochem. **55:**663–700.
29. **Michels, P. A. M., N. Chevalier, F. R. Opperdoes, M. H. Rider, and D. J. Rigden.** 1997. The glycosomal ATP-dependent phosphofructokinase of *Trypanosoma brucei* must have evolved from an ancestral pyrophosphate-dependent enzyme. Eur. J. Biochem. **250:**698–704.
30. **Moreno, S. N. J., and L. Zhong.** 1996. Acidocalcisomes in *Toxoplasma gondii* tachyzoites. Biochem. J. **313:**655–659.
31. **Ochoa, S.** 1955. Isocitric deshydrogenase system (TPN) from pig heart. Methods Enzymol. **1:**699–704.
32. **Padh, H., M. Lavasa, and T. L. Steck.** 1991. Endosomes are acidified by association with discrete proton-pumping vacuoles in *Dictyostelium*. J. Biol. Chem. **266:**5514–5520.
33. **Rea, P. A., and R. J. Poole.** 1993. Vacuolar $H^+$-translocating pyrophosphatase. Annu. Rev. Plant Physiol. Plant Mol. Biol. **44:**157–180.
34. **Rodrigues, C. O., D. A. Scott, and R. Docampo.** 1999. Presence of a vacuolar $H^+$-pyrophosphatase in promastigotes of *Leishmania donovani* and its localization to a different compartment from the vacuolar $H^+$-ATPase. Biochem. J. **340:**759–766.
35. **Scott, D. A., S. N. J. Moreno, and R. Docampo.** 1995. $Ca^{2+}$ storage in *Trypanosoma brucei*: the influence of cytoplasmic pH and importance of vacuolar acidity. Biochem. J. **310:**780–794.
36. **Scott, D. A., and R. Docampo.** 1998. Two types of $H^+$-ATPase are involved in the acidification of internal compartments in *Trypanosoma cruzi*. Biochem. J. **331:**583–589.
37. **Scott, D. A., R. Docampo, J. A. Dvorak, S. Shi, and R. D. Leapman.** 1997. In situ compositional analysis of acidocalcisomes in *Trypanosoma cruzi*. J. Biol. Chem. **272:**28020–28029.
38. **Scott, D. A., W. de Souza, M. Benchimol, L. Zhong, H.-G. Lu, S. N. J. Moreno, and R. Docampo.** 1998. Presence of a plant-like proton-pumping pyrophosphatase in acidocalcisomes of *Trypanosoma cruzi*. J. Biol. Chem. **273:**22151–22158.
39. **Solioz, M.** 1984. Dicyclohexylcarbodiimide as a probe for proton translocating enzymes. Trends Biochem. Sci. **9:**309–312.
40. **Steiger, R. F., F. R. Opperdoes, and J. Bontemps.** 1980. Subcellular fractionation of *Trypanosoma brucei* bloodstream forms with special reference to hydrolases. Eur. J. Biochem. **105:**163–175.
41. **UNDP/World Bank/WHO Special Programme for Research and Training in Tropical Diseases.** 1997. Tropical disease research: progress 1995–1996: thirteenth programme report of the UNDP/World Bank/WHO Special Programme for Research and Training in Tropical Diseases. World Health Organization, Geneva, Switzerland.
42. **Vercesi, A. E., S. N. J. Moreno, and R. Docampo.** 1994. $Ca^{2+}/H^+$ exchange in acidic vacuoles of *Trypanosoma brucei*. Biochem. J. **304:**227–233.
43. **Vercesi, A. E., and R. Docampo.** 1996. Sodium-proton exchange stimulates $Ca^{2+}$ release from acidocalcisomes of *Trypanosoma brucei*. Biochem. J. **315:**265–270.
44. **Vercesi, A. E., M. Grijalba, and R. Docampo.** 1997. Inhibition of $Ca^{2+}$ release from *Trypanosoma brucei* acidocalcisomes by 3,5-dibutyl-4-hydroxytoluene: role of the $Na^+/H^+$ exchanger. Biochem. J. **328:**479–482.
45. **Vickerman, K., and L. Tetley.** 1977. Recent ultrastructural studies on trypanosomes. Ann. Soc. Belge Med. Trop. **57:**441–455.
46. **Waggoner, A. S.** 1988. Mechanisms of membrane potential probes, p. 211–215. *In* R. Gunn and J. L. Parker (ed.), Cell physiology of blood, The

Rockefeller University Press, New York, N.Y.
47. **Wang, Y., R. A. Leigh, K. H. Kaestner, and H. Sze.** 1986. Electrogenic $H^+$-pumping pyrophosphatase in tonoplast vesicles of oat root. Plant Physiol. **81:**497–502.
48. **Webb, M. R.** 1992. A continuous spectrophotometric assay for inorganic phosphate and for measuring phosphate release kinetics in biological systems. Proc. Natl. Acad. Sci. USA **89:**4884–4887.
49. **Williamson, J., and D. J. McLaren.** 1981. Localization of phosphatases in *Trypanosoma rhodesiense*. J. Protozool. **28:**460–467.
50. **Zhen, R.-G., A. A. Baykov, N. P. Bakuleva, and P. A. Rea.** 1994. Aminomethylenediphosphonate: a potent type-specific inhibitor of both plant and phototrophic bacterial $H^+$-pyrophosphatases. Plant Physiol. **104:**153–159.